On the basis of these principles, we classified major tragal malformations into 3 types according to the morphology of the deformed tragal cartilage and its connection to the AA and EAC cartilages. In ~50% of cases (type I), the tragal cartilage exhibited a typical triangular shape resembling normal anatomy and was naturally connected to the AA and EAC cartilages. In the remaining cases, the tragal cartilage was either atypical and distorted (type II) or rudimentary (type III), with abnormal connection to the AA and EAC cartilages. This classification system provides a framework for selecting appropriate surgical strategies for anatomic tragal reconstruction.

The primary surgical goal in treating major tragal malformation was to reconstruct the 3 cartilage components into a laminated cartilage plate that mimics the normal structure of the outer and inner frameworks. In all types, repositioning the EAC cartilage using traction and bending suture techniques was essential to restore the inner framework before reconstructing the outer framework. The method for reconstructing the outer framework depended entirely on the morphology of the tragal cartilage. In type I cases, a cartilage transposition flap of the typical tragal cartilage was used. In type II and III cases, the atypical or rudimentary tragal cartilage was excised from the EAC cartilage, and the outer framework was reconstructed using a free cartilage graft harvested from the excised AA and/or tragal cartilage. Therefore, preservation of the tragal cartilage and the assessment of its availability during skin flap elevation and perichondral dissection are crucial for surgical planning.

The secondary surgical goal was to achieve natural soft tissue contour and adequate coverage of the reconstructed cartilage framework without skin defects or scar-related deformities. The TP normally has thick soft tissues, whereas the STR and ITR have thin coverage. However, the posterior skin flap used during surgery was typically thinner than that of the native TP. When soft tissue was insufficient over the ridge-top cartilage of the reconstructed tragus, complications such as small TP and/or cartilage visibility occurred due to skin thinning. To prevent this, we performed soft tissue augmentation using a fascial graft over the ridge-top cartilage and closed the wound in a T-shape. T-shape closure, achieved through triangular wedge excision and marginal folding of the posterior skin flap before the TP, was particularly effective in maintaining soft tissue volume and projection. In addition, placing the anterior incision line along the preauricular groove facilitated scar management with skin taping and made the scar less conspicuous.

These surgical techniques proved effective even in cases where the main body of the AA was previously excised (Supplementary Digital Content, Fig. 2, http://links.lww.com/SCS/J84). In such cases, the deformed tragal cartilage and part of the AA cartilage were frequently retained, allowing for outer framework reconstruction using either a cartilage transposition flap or a free graft without the need for additional cartilage harvesting.

CONCLUSIONS

This structural analysis and classification system, based on 3 consistently deformed cartilage components, provides new insights and surgical guidelines for total tragal reconstruction. The inner framework is restored through anatomic repositioning of the EAC cartilage, and the outer framework is reconstructed using either a cartilage transposition flap or a free cartilage graft derived from the tragal and/or AA cartilage. The newly formed framework is then covered with a posterior skin flap to achieve a natural external contour. This approach emphasizes the pivotal role of the tragal cartilage—rather than the AA cartilage—in surgical planning for achieving anatomic reconstruction. These findings may help optimize the restoration of a natural tragal contour with minimal scarring. Furthermore, this study offers valuable contributions to understanding the pathologic anatomy and embryology of major tragal malformations.

ACKNOWLEDGMENTS

The authors are sincerely grateful to the Medtube manager for granting permission to reproduce the auricular cartilage photograph of Michael Hawke shown in Figure 1.

REFERENCES

1. Komune N, Fukushima J, Rhoton AL Jr. Auricle and external acoustic meatus. *Anatomy for Plastic Surgery of the Face, Head, and Neck*. New York: Thieme (eBook); 2016: 161–171. Accessed February 3, 2018. https://search.ebscohost.com/login.aspx?direct = true&db = nlebk&AN = 1246630&site = ehost-live
2. Sullivan RF. Auricular cartilage. The auricle: pinna/concha. Accessed December 11, 2014. http://www.rcsullivan.com/www/pinna.htm
3. Hawke M. The auricular cartilage. Accessed October 11, 2023. https://medtube.net/otorhinolaryngology/medical-images/29547-the-auricular-cartilage.
4. Parisier S. Cadaver dissection of auricular cartilage. The meatus and cavity management. Accessed March 4, 2022. https://entokey.com/the-meatus-and-cavity-management/
5. Hwang J, Cho J, Burm JS. Accessory auricle: classification according to location, protrusion pattern and body shape. *Arch Plast Surg* 2018;45:411–417
6. Streeter GL. Development of the auricle in the human embryo. *Contributions to Embryology*. Washington DC: Carnegie Institution of Washington; 1922;14:111–138
7. Davis J. *Aesthetic and Reconstructive Otoplasty*. New York: Springer; 1987:93–125
8. Chen Y, Wei S, Hao D, et al. Reconstruction of the deformed tragus accompanied by accessory auricle. *Aesthet Surg J* 2023;43: NP687–95
9. Li Q, Sheng Y, Jiang Z, et al. Practical classification and management of accessory auricle. *Aesthet Plast Surg* 2024;48: 1653–1662
10. Park C. Reconstruction of congenital tragal malformations accompanied by dystopic cartilage growth (accessory tragus). *Plast Reconst Surg* 2015;135:1681–1691
11. Jeon JI, Ha JH, Kim S. Chondrocutaneous transposition flap for congenital tragal malformation with dystrophic cartilage. *Arch Craniofac Surg* 2019;20:405–407
12. Mei A, Li T, Qiu L, et al. Cartilage transposition and anchoring: a surgical technique for the reconstruction of congenital tragal malformation in children. *J Plast Reconst Aesthet Surg* 2023;82: 229–234

OPEN

Computer-Guided Biopsy of Osteosclerotic Jaw Lesion Using 3D-Printed Surgical Guides: A Fully Digital Workflow

Pierluigi Mariani, DDS, Diana Russo, DDS, PhD,**
Francesco Rullo, DDS, Lucio Lo Russo, DDS,†*
Angelo Salamini, DES,‡ Vincenzo Ronsivalle,§
*Marco Cicciù, DDS, PhD,§ and Luigi Laino, DDS, PhD**

Abstract: Osteosclerotic jaw lesions, often incidentally detected on routine radiographs, are rarely biopsied due to their benign appearance and proximity to delicate anatomic structures. This case report presents a fully digital workflow for guided biopsy of a deep mandibular osteosclerotic lesion, integrating artificial intelligence-based segmentation, intraoral scanning, CAD design, and 3D printing of surgical templates. A 3D-printed guide with depth-control stops was used to safely and precisely position trephine burs between the roots of tooth 4.6 and the mandibular canal. The approach allowed accurate tissue sampling for histopathologic diagnosis (osteoma), minimizing invasiveness and risk to adjacent structures. Postoperative CBCT confirmed the accuracy of the biopsy, with deviations of 0.6 mm (linear), 4 degrees (angular), and −0.2 mm (depth). This technique demonstrates the potential of artificial intellingence-assisted digital planning and 3D printing to enhance biopsy precision for intraosseous lesions.

Key Words: 3D-printed surgical guide, AI-based CBCT segmentation, computer-guided biopsy, fully digital workflow, osteosclerotic jaw lesions

Asymptomatic osteosclerotic lesions, often incidentally detected during routine radiographic examinations, are rarely investigated further due to their usually benign nature, particularly when they are near critical anatomic structures. This approach may result in these lesions remaining without a definitive diagnosis or being classified solely based on a presumptive radiographic interpretation.

From the *Multidisciplinary Department of Medical-Surgical and Odontostomatological Specialties, University of Campania, “Luigi Vanvitelli”, Naples; †Department of Clinical and Experimental Medicine, School of Dentistry, University of Foggia, Foggia; ‡R&D Manager Evolab, Caserta; and §Department of General Surgery and Surgical-Medical Specialties, School of Dentistry, University of Catania, Catania, Italy.
Received December 17, 2025.
Accepted for publication January 6, 2026.
Address correspondence and reprint requests to Marco Cicciù, DDS, PhD, Department of General Surgery and Surgical-Medical Specialties, School of Dentistry, University of Catania, Via Santa Sofia 78, 95123, Catania, Italy; E-mail: marco.cicciu@unict.it
The research leading to these results has received funding from the European Union-NextGenerationEU through the Italian Ministry of University and Research under PNRR-M4C2-I1.3 Project PE_00000019 “HEAL ITALIA” to Marco Cicciù CUP E63C22002080006. The views and opinions expressed are those of the authors only and do not necessarily reflect those of the European Union or the European Commission. Neither the European Union nor the European Commission can be held responsible for them.
The authors report no conflicts of interest

ISSN: 1536-3732
DOI: 10.1097/SCS.0000000000012501

Performing an incisional biopsy on such lesions can be challenging, both due to their location and the complex anatomy of the maxillofacial region, which is characterized by delicate structures such as the inferior alveolar nerve and dental roots.[1] In this context, 3-dimensional (3D) printed surgical guides may represent valuable tools to enhance biopsy accuracy and ensure the precise collection of tissue samples for histological analysis.[2–4]

The 3D printing is already widely used in oral and maxillofacial surgery, particularly in implantology, where the use of surgical guides has become standard practice.[5] However, with regard to jawbone pathologies, the current literature remains limited and fragmented. A recent systematic review,[6] aimed at evaluating the contribution of CAD/CAM technology to the surgical management of jaw cysts and tumors, included only 13 studies, of which only one was a randomized clinical trial (RCT). The findings revealed that 3D printing has mainly been utilized for the fabrication of anatomic models for preoperative planning and visualization, as well as for educational purposes. Only 8 studies reported the intraoperative use of surgical guides, mainly for intraoperative osteotomy and, in fewer cases, for intraoperative drilling location, whereas a single study described the application of 3D-printed postoperative devices for the marsupialization of osteolytic lesions.[7] More recent studies have provided preliminary data on the accuracy of guided biopsies compared with freehand approaches, highlighting the superior precision of the former.[8,9] Nonetheless, to date, the literature does not yet provide a detailed, standardized, and reproducible protocol for fully digital surgical planning. The aim of this paper is to clearly and in detail report the full digital workflow for performing computer-guided biopsies of osteosclerotic lesions.

MATERIALS AND METHODS

A 38-year-old man was referred by the dentist to the Department of Oral Surgery of the University of Campania Luigi Vanvitelli to investigate the nature of an osteosclerotic lesion, localized at the level of teeth 4.5 and 4.6, having relationships with the apices of these teeth and apically had relationships with the mandibular canal (MC) (Fig. 1).

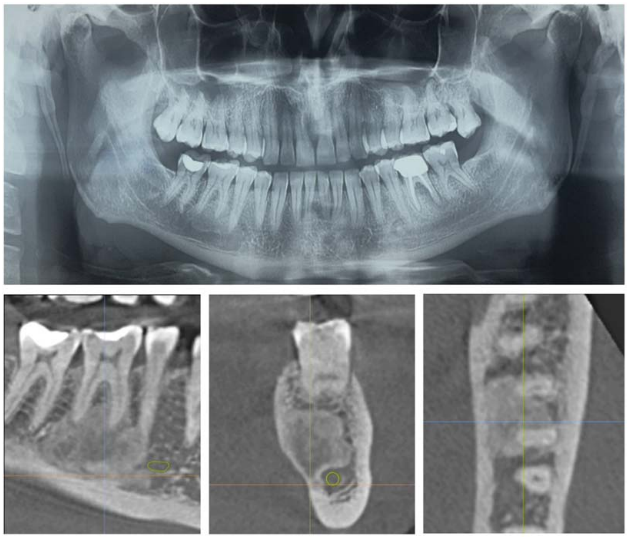

FIGURE 1. Radiographic images: orthopantomography, and coronal, axial, and panorex CBCT sections of the osteosclerotic lesion.

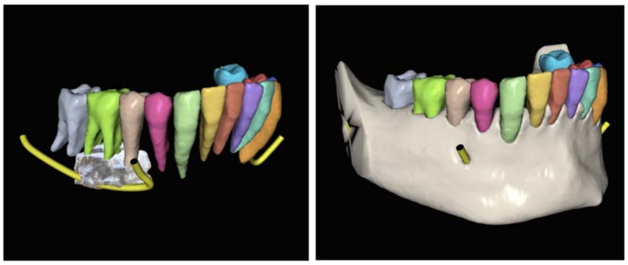

FIGURE 2. The automatic segmentation function using artificial intelligence.

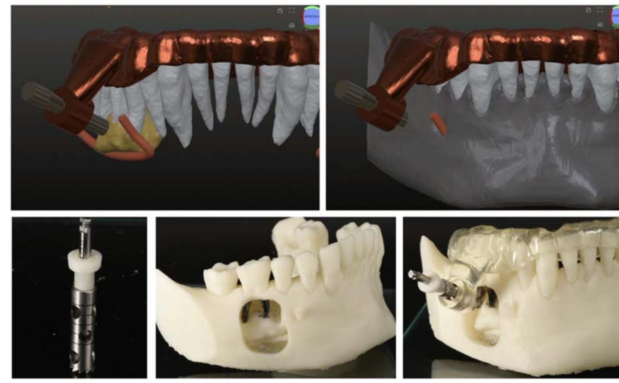

FIGURE 4. Evaluation of correct planning of the template and correct orientation of the bur using Nomad Sculpt software. A 3D-printed surgical stop drill, and a 3D stereolithography model with an inspection hatch were printed to evaluate the planning quality in the pre-clinical phase.

The area chosen for biopsy was between the roots of tooth 4.6 and coronal to the MC. The use of 2 coaxial trephine burs was planned, one 5 mm in external diameter and the other 4 mm. (Meisinger T229L-080-RAL and 229L-030-RAL; Hager & Meisinger GmbH).

Using Blue Sky Plan software [Blue Sky Bio, LLC. (2025). *Blue Sky Plan* (Dental treatment planning software)],[10] the intraoral scan (STL) file was aligned with the DICOM data from the Cone Beam computed tomography analysis [Orthopos SL (Dentsply Sirona)]. The automatic segmentation function using Artificial Intelligence (AI) was used to segment the mandibular bone, the teeth, and the MC (Fig. 2). The osteosclerotic lesion to be analyzed was manually segmented by applying a filter related to the range between a maximum and minimum gray value according to the Hounsfield scale.

An STL file of each component was then obtained, useful for the case study. Obtaining individual files of the different components was useful for surgical planning as it allowed for selective visualization of each component. The chosen trephine burs were designed in 3D using Rhinoceros CAD [Robert McNeel & Associates. *Rhinoceros* (software): Robert McNeel & Associates; 2025].

All files were loaded into Nomad Sculpt software [Ginier S. *Nomad Sculpt* (software): Stéphane Ginier; 2025]. Nomad Sculpt was used for its advanced visualization functions and for better management of movements and rotations between files. The direction and depth of the trephine burs entry were established, also considering the use of an extension (Fig. 3). Once the final position of the burs was validated, all files were exported in position and loaded into 3Shape Appliance Designer software [3Shape A/S. *3Shape Appliance Designer* (software); 2025] (Fig. 3). This kind of support can also be printed by the Form4BL 3D printer (Formlabs Inc.)

The portion of the template relating to the dental support was created using the "create shell" function. An offset was applied to improve the passivity of the support and to eliminate any undercuts.

A solid cylinder was created at the burs' location using Boolean subtraction with the burs CAD previously designed and positioned in Nomad Sculpt to form the sleeves.

The resulting sleeves were connected to the tooth-supporting portion using the bar function. The intraoral scan model was subtracted from the Boolean connection between the tooth-supporting portion, the sleeve, and the bar to eliminate any interference with the mucosa and the fornices.

To ensure that the drilling stopped at the planned depth, 2 rings (different for the 2 burs) were created using Rhinoceros CAD [Robert McNeel & Associates. *Rhinoceros* (software): Robert McNeel & Associates; 2025] to prevent further advancement of the drill upon contact with the sleeve. The 2 templates thus produced were made using addition technology using a 3D stereolithography printer with a laser-based UV light source [*SprintRay Surgical Guide 3.* SprintRay Inc. (2025)] (Fig. 4).

After the administration of local anesthesia, a marginal mucoperiosteal envelope flap was performed with exposure of the posterior mandibular body. This approach was necessary to allow deeper placement of the 3D-printed surgical guide, due to the deep location of the lesion and because, during maximal mouth opening, the vestibular fold caused displacement and instability of the template.

Once the guide was properly positioned on the mandibular arch, bone trepanation was carried out using a first trephine bur to the predetermined depth, aided by a mechanical stop. A second trephine was then used to core out the lesion. The bone specimen was fractured and removed, then sent to the pathology

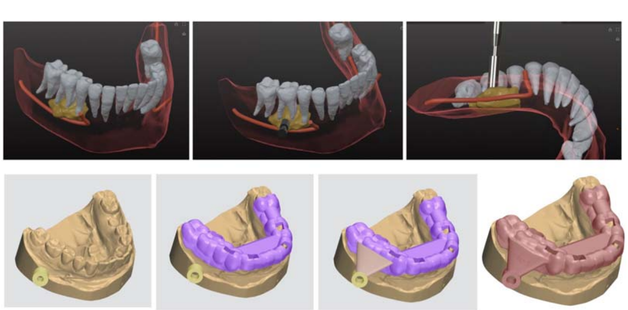

FIGURE 3. Digital planning using the CAD design of the bur imported along with all the anatomic components into Nomad Sculpt software. Design of the surgical guide and bur sleeve using 3Shape Appliance Designer software.

FIGURE 5. Surgical workflow of a guided biopsy

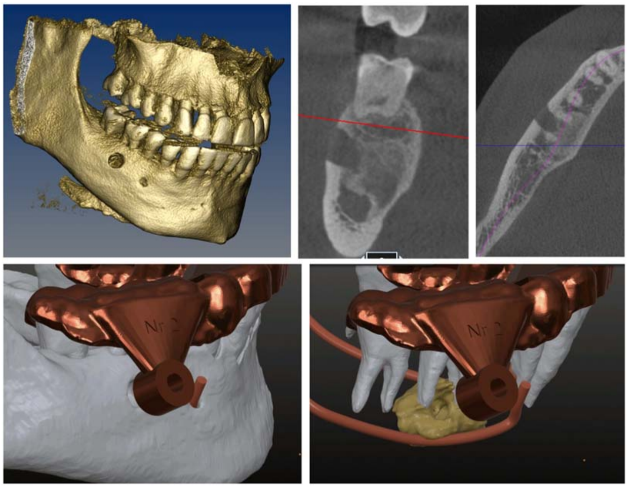

FIGURE 6. Postoperative CBCT in axial and coronal plane shows the correct removal of the pathologic tissue and the respect of the roots of tooth 4.6 and the mandibular canal. The 3D reconstruction highlights the entrance foramen. The visualization of the 3D reconstruction imported into Nomad Sculpt software demonstrates the consistency between digital planning and surgical execution.

department for histopathologic examination, which confirmed the diagnosis of osteoma (Fig. 5).

At the end of the procedure, the surgical site was irrigated, hemostasis was achieved, and the soft tissues were closed primarily using non-resorbable silk sutures. A postoperative CBCT confirmed a safe distance between the bone window, the mandibular canal, and the roots of tooth 4.6 (Fig. 6). The postoperative course was uneventful, with no signs of hypoesthesia or paresthesia of the lower lip, nor any other reported complaints.

DISCUSSION

The use of AI for the segmentation of the mandibular structure and the lesion, combined with digital impressions and dedicated design software, enabled the straightforward, and predictable fabrication of surgical guides. These guides assist the clinician in performing biopsies that would otherwise be highly invasive,[11] requiring an excessive sacrifice of biological tissues both in terms of flap size and the amount of bone removed and carrying a high risk of injury to the inferior alveolar nerve or the roots of adjacent teeth involved in the lesion.

Recent studies have evaluated the accuracy of such guided biopsies, including one in vitro study[8] and 2 clinical studies.[3,9] All of them consistently report that surgical guides produced using desktop stereolithographic 3D printers allow for significantly higher accuracy in biopsy procedures.

The planning and design of the depth-control stops allowed for the collection of an adequate biopsy specimen, enabling the pathology department to perform a reliable histopathologic evaluation. In cases of osteosclerotic lesions, it can be challenging to harvest a sufficient amount of pathologic tissue due to the clinical similarity between bone tissue and the pathologic tissue, particularly when the lesion is located near delicate anatomic structures.

In the current surgical plan, the decision was made to use 2 coaxial trephine burs—one with an external diameter of 5 mm and the other with an external diameter of 4 mm. This choice was made for 2 main reasons: first, to increase the thickness of the osteotomy line, thus facilitating more apical positioning of the instrument to allow adequate fracture of the entire sample (given that it had different densities represented by cortical bone, medullary bone, and osteosclerotic lesion); second, because as one penetrated deeper into the lesion, the space became increasingly narrower (between the roots and MC), so only the 4 mm bur was brought to working length for lesion sampling, whereas the 5 mm bur remained 4 mm more superficial.

Postoperative CBCT imaging was used to assess the quality of the biopsy and to measure the discrepancy between the planned and the actual position of the biopsy channel. The results demonstrated good accuracy: the linear deviation of the cylinder axis was 0.6 mm, the angular deviation was 4 degrees, and the depth deviation was −0.2 mm.

Although minimal, these deviations may be attributed to cumulative errors occurring throughout the digital workflow—from segmentation and design to the fabrication of the surgical guide—as well as to slight flexion of the guide under pressure during the use of the rotary handpiece.

REFERENCES

1. Peditto M, Nucera R, Rubino E, et al. Improving oral surgery: a workflow proposal to create custom 3D templates for surgical procedures. *Open Dent J* 2020;14:35–44
2. Omara M, Gouda A, Ali S. Computer-guided buccal cortical plate separation for removal of calcified benign odontogenic tumors affecting the mandibular angle region. *Maxillofac Plast Reconstr Surg* 2022;44:30
3. Lotz M, Schumacher C, Stadlinger B, et al. Accuracy of guided biopsy of the jawbone in a clinical setting: a retrospective analysis. *J Craniomaxillofac Surg* 2021;49:556–561
4. Van Hoe S, Shaheen E, de Faria Vasconcelos K, et al. Contribution of three-dimensional images in the planning of cementoblastoma resection. *BJR Case Rep* 2021;7:20200156
5. Lo Russo L, Mariani P, Zhurakivska K, et al. Three-dimensional accuracy of surgical guides for static computer-aided implant surgery: a systematic review. *Prosthesis* 2023;5:809–825
6. Gernandt S, Tomasella O, Scolozzi P, et al. Contribution of 3D printing for the surgical management of jaws cysts and benign tumors: a systematic review of the literature. *J Stomatol Oral Maxillofac Surg* 2023;124:101433
7. Kivovics M, Penzes D, Moldvai J, et al. A custom-made removable appliance for the decompression of odontogenic cysts fabricated using a digital workflow. *J Dent* 2022;126:104295
8. Postl L, Mucke T, Hunger S, et al. In-house 3D-printed surgical guides for osseous lesions of the lower jaw: an experimental study. *Eur J Med Res* 2021;26:25
9. Postl L, Mucke T, Hunger S, et al. Biopsies of osseous jaw lesions using 3D-printed surgical guides: a clinical study. *Eur J Med Res* 2022;27:104
10. Lo HY, Leung PH, Su YX, et al. AI-driven CBCT segmentation and 3D modeling of the anterior surface of maxilla for computer-assisted surgery: a comparison of multiple algorithms. *J Craniomaxillofac Surg* 2025;53:1683–1690
11. Hu YK, Xie QY, Yang C, et al. Computer-designed surgical guide template compared with free-hand operation for mesiodens extraction in premaxilla using "trapdoor" method. *Medicine (Baltimore)* 2017;96:e7310

Parietal Intradiploic Epidermoid Cyst Invading the Dura Mater